SAND2014-16997J

Photoionization mass spectrometric measurements of initial reaction pathways in low-temperature oxidation of 2,5-dimethylhexane

Brandon Rotavera[1], Judit Zádor[1], Oliver Welz[1#], Leonid Sheps[1], Adam M. Scheer[1], John D. Savee[1], Mohamad Akbar Ali[2], Taek Soon Lee[3], Blake A. Simmons[3,4], David L. Osborn[1], Angela Violi[2], and Craig A. Taatjes[1]

[1]Combustion Chemistry Department, Combustion Research Facility, *Sandia National Laboratories*, Livermore, CA 94550-0969, United States
[2]Department of Mechanical Engineering, *University of Michigan*, Ann Arbor, MI 48109-2125, United States
[3]Joint BioEnergy Institute, Emeryville, CA 94608, United States
[4]Biofuels and Biomaterials Science and Technology Department, *Sandia National Laboratories*, Livermore, CA 94551, United States
[#]Present address: Institute for Combustion and Gas Dynamics – Reactive Fluids, University of Duisburg-Essen, Duisburg, Germany

Abstract

Alkylperoxy (ROO) decomposition pathways relevant to low-temperature autoignition chemistry were studied for 2,5-dimethylhexane, a symmetrically branched octane isomer, at 550 K and 650 K using Cl-atom initiated oxidation and multiplexed photoionization mass spectrometry (MPIMS). Interpretation of time- and photon-energy-resolved mass spectra led to three specific results important to characterizing the initial oxidation steps: (1) quantified isomer-resolved branching ratios for HO_2 + alkene channels; (2) 2,2,5,5-tetramethyl-tetrahydrofuran is formed substantial yield from addition of O_2 to tertiary 2,5-dimethylhex-2-yl followed by isomerization of the resulting ROO adduct to tertiary QOOH, and exhibits a positive dependence on temperature over the range covered leading to a higher flux relative to aggregate cyclic ether yield. The higher relative flux is explained by a 1,5-hydrogen atom shift reaction that converts the initial primary alkyl radical (2,5-dimethyl-1-hexyl) to the tertiary alkyl radical 2,5-dimethyl-2-hexyl, providing an additional source of tertiary alkyl radicals. Quantum-chemical and master-equation calculations of the unimolecular decomposition of the primary alkyl radical reveal that isomerization to the tertiary alkyl radical is the most favorable pathway, and is favored over O_2-addition at 650 K under the conditions herein. The isomerization pathway to tertiary alkyl radicals therefore contributes an additional mechanism to 2,2,5,5-tetramethyl-tetrahydrofuran formation; (3) carbonyl species (acetone, propanal, and methylpropanal) consistent with β-scission of QOOH radicals were formed in significant yield, indicating unimolecular QOOH decomposition into carbonyl + alkene + OH.

Keywords: octane isomer, 2,2,5,5-tetramethyl-tetrahydrofuran, bisabolane, autoignition chemistry, photoionization mass spectrometry

1. Introduction

Branched alkanes are common species in conventional transportation fuel [1] and some bio-derived fuels, including microbially-derived sesquiterpenoid fuels produced by fermentation [2]. 2,5-dimethylhexane is a symmetrically branched octane isomer similar to constituents in renewable jet fuel [3], and is also part of a component-centered approach to understanding low-temperature oxidation of structurally complex fuel molecules by examining oxidation of smaller molecules that are structural motifs of the larger, targeted fuel molecule. In general, increased branching in alkanes is associated with diminished low-temperature reactivity [4] due to the increasing number of primary C–H bonds. Abstraction of primary hydrogen in ROO (alkyl peroxy) ⟶ QOOH (hydroperoxyalkyl) isomerization has a higher barrier than abstraction of secondary or tertiary hydrogen due to the stronger primary C–H bond. Higher barriers to H-abstraction inhibit QOOH formation and, by extension, chain-branching which governs autoignition. Low-temperature oxidation studies on linear and mono-methylated alkanes (primarily *iso*-alkanes/2-methyl-alkanes) of carbon number > 7 are common. However, only limited prior work [5] and sparse recent work focuses on the oxidation chemistry of di-methylalkanes [6, 7].

The effects of alkane structure on chain-branching reactions, from linear to tetramethyl-substituted alkanes ranging from C_4 to C_{10}, were studied analytically by Morley [5]. Arrhenius rate parameters for H-atom transfer reactions in alkylperoxy radicals from Baldwin et al. [8] were employed in [5] to calculate average rates of chain-branching, marked by species leading to the formation of OH initiated by ROO isomerization. Results were calculated in [5] for a series of octane isomers using a reference temperature of 750 K and indicated that the rate of OH production from 2,5-dimethylhexane oxidation is less than half that of *n*-octane, yet nearly a factor of four higher than the rate from *iso*-octane, reflecting a trend of higher reactivity of less-branched alkanes. It is noteworthy that the assumptions in [5] lead to an upper limit on chain-branching from OOQOOH due to neglect of interaction of carbon-bound O atoms with neighboring H atoms and neglect of the potential for a concerted reaction step (i.e. OOQOOH → OQ=O + 2OH). Theoretical calculations were conducted in Pfaendtner et al. [6] on transition state geometries and energy barriers to intramolecular hydrogen abstraction for a range of linear and branched ROO species, including radicals derived from 2,5-dimethylhexane, and lead to the result that ROO ⟶ QOOH isomerization reactions via 1,5-H shifts were favored for branched alkanes. Miyoshi conducted a generalized treatment of alkyl substituent effects in noncylic alkanes on unimolecular reactions of ROO and of QOOH using CBS-QB3 [9], and Villano et al. derived rate rules for R + O_2 reactions of alkanes [10, 11]. Species profiles from jet-stirred reactor experiments, measured from 550 – 1150 K, and shock-tube ignition delay times were utilized to compare with predictions from a comprehensive chemical kinetics mechanism developed for 2,5-dimethylhexane [7]. The ignition delay times of octane isomers in

Sarathy et al. [7] were measured in air from 850 K to 1300 K at 20 atm, and 2,5-dimethylhexane displayed ignition times longer than for *n*-octane by a factor of approximately five, again reflecting the inhibiting influence of alkane branching on autoignition.

Branching is also common in biofuels, and 2,5-dimethylhexane represents a component analog to several bio-derived species (e.g. bisabolane and 1-methyl-4-*iso*-propylcyclohexane [2]). Therefore, characterizing the oxidation tendencies of branched alkanes contributes to fundamental insight into the oxidation of more-complex biofuels. Accordingly, to complement the existing studies on low-temperature oxidation of di-methylalkanes, the present study focuses on fundamental characterization of the initial oxidation steps of 2,5-dimethylhexyl radicals (R) with O_2, the details of which are important in deriving accurate chemical kinetic mechanisms of low-temperature autoignition, as discussed in Zádor et al. [12], Taatjes [13], and Battin-Leclerc [14]. The complexity of R + O_2 reactions lies in the numerous competing pathways the ROO adduct and subsequent QOOH radicals undergo, and the contribution from both formally direct (i.e. well-skipping) and sequential channels to product formation [12]. Low-temperature oxidation of alkanes follows a degenerate chain-branching scheme (Fig. 1), and the present study focuses on product formation from R + O_2: conjugate alkene + HO_2, cyclic ether + OH, and QOOH decomposition channels via C–C β-scission.

The competition among channels from R + O_2 determines autoignition behavior. Because HO_2 is unreactive at low temperature (< ~900 K), and because the dominant HO_2 removal reactions lead primarily to hydrogen peroxide (H_2O_2) which is stable at low temperatures, channels leading to HO_2 + conjugate alkene are effectively chain-terminating at low temperature. Cyclic ether formation channels are chain-propagating because of the coincident formation of a reactive OH radical. Isomeric resolution of cyclic ethers is important to combustion modeling because it allows determination of specific QOOH pathways. QOOH radicals are critical to autoignition because the addition reaction QOOH + O_2 → OOQOOH (termed second O_2-addition) eventually leads to low-temperature chain-branching. The second O_2-addition reactions must compete with decomposition or isomerization of QOOH species. The characteristics of conjugate alkene formation, cyclic ether formation, and species related to C–C *β*-scission of QOOH radicals determine the initial steps of low-temperature autoignition and are the focus of the present study.

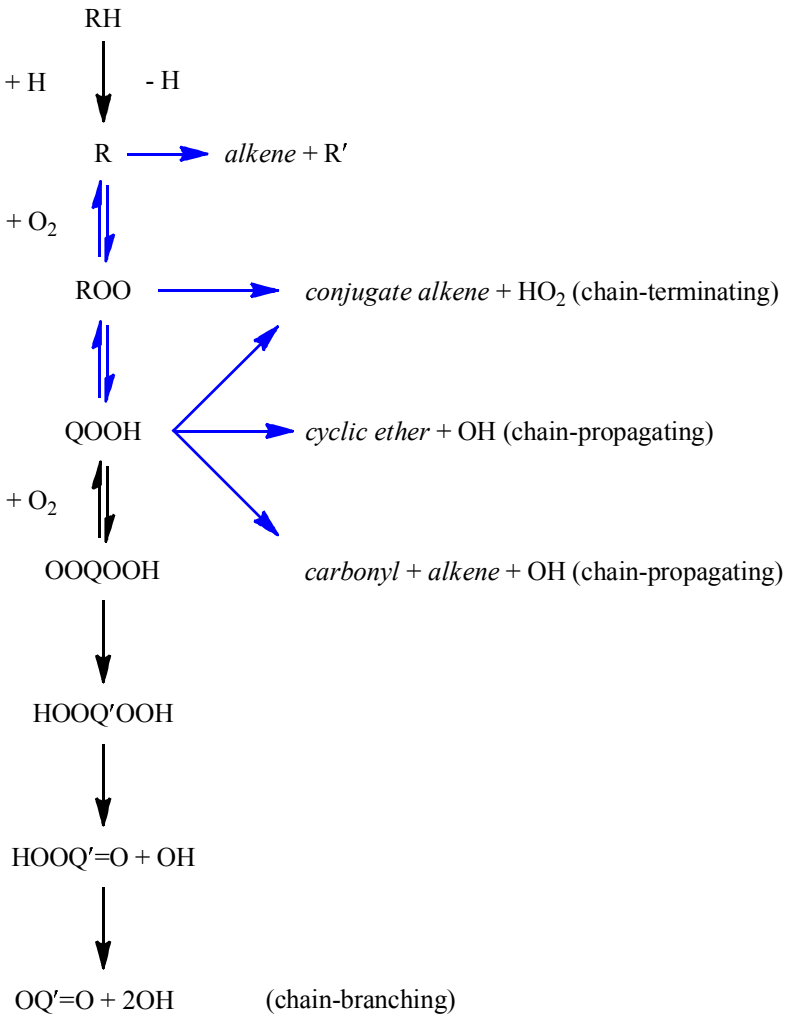

Fig. 1. Generalized low-temperature alkane oxidation mechanism (coloring indicates the set of reactions of interest and italicized species were measured directly).

2. Experimental and computational methods

2.1. Experimental methods

Oxidation experiments at 550 K and 650 K were performed at the Chemical Dynamics Beamline of the Advanced Light Source (ALS) synchrotron [15, 16] using the Multiplexed Photoionization Mass Spectrometry (MPIMS) apparatus described in Osborn et al. [17], retrofitted with an orthogonal-acceleration time-of-flight mass spectrometer [18, 19]. The synchrotron provides quasi-continuous, tunable vacuum ultraviolet (VUV) light for photoionization. The MPIMS apparatus contains a resistively heated, slow-flow quartz reactor (62-cm length, 1.05-cm inner diameter) through which a flow of 2,5-dimethylhexane, O_2, and Cl_2 highly diluted in He, was maintained at constant pressure (8 Torr). Flow rates during the experiments were set such that the volume inside the reactor was completely replenished between subsequent 4-Hz photolysis-laser pulses. To initiate the reaction, Cl_2 was photolyzed by a 351-nm excimer laser generating Cl atoms that abstract H atoms from 2,5-dimethylhexane (RH) yielding initial fuel radicals R (Fig. 2). Three structurally distinct alkyl radicals are produced as a result of H-abstraction by Cl (Fig. 2). Because of the low site-selectivity of chlorine atoms, all three 2,5-dimethylhexyl radical isomers are formed.

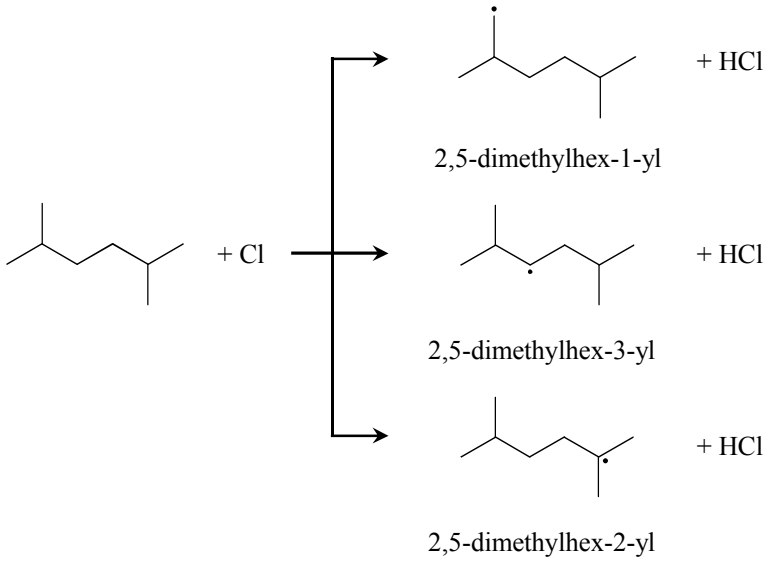

Fig. 2. Initial alkyl radicals formed by H-abstraction from 2,5-dimethylhexane by Cl atoms. The symmetry of 2,5-dimethylhexane limits the number of structurally-distinct initial radicals to three: primary R (2,5-dimethylhex-1-yl), secondary R (2,5-dimethylhex-3-yl), and tertiary R (2,5-dimethylhex-2-yl).

To estimate the initial distribution of alkyl radicals from the 2,5-dimethylhexane + Cl reaction, branching ratios were calculated at 550 K and 650 K following the structure-activity relationship (SAR) methodology of Atkinson [20]. Using SAR for 2,5-dimethylhexane at 296 K, and assuming a weak dependence on temperature [21], a total rate coefficient of $2.6 \cdot 10^{-10}$ cm^3 molecule^{-1} s^{-1} is predicted at both 550 K and 650 K. Branching ratios for H-abstraction from primary, secondary, and tertiary sites by Cl were then derived using trends for primary and secondary sites from propane [22] and for tertiary site abstraction from *iso*-butane + Cl → *tert*-butyl + HCl [23] (Table 1).

Table 1. Site-specific rate coefficients (cm^3 molecule^{-1} · s^{-1}) and branching fractions for the 2,5-dimethylhexane + Cl reaction calculated using SAR. Rate coefficients represent total values.

Temperature	2,5-dimethyl-hex-1-yl (primary R)	2,5-dimethyl-hex-3-yl (secondary R)	2,5-dimethyl-hex-2-yl (tertiary R)
550 K	$1.21 \cdot 10^{-10}$	$9.26 \cdot 10^{-11}$	$6.12 \cdot 10^{-11}$
	44%	34%	22%
650 K	$1.23 \cdot 10^{-10}$	$9.05 \cdot 10^{-11}$	$6.12 \cdot 10^{-11}$
	45%	33%	22%

Mole fractions and number densities utilized in the experiments are listed in Table 2. Approximately 3% of Cl is formed from 351-nm photolysis of Cl_2. The high $[O_2]:[R]_0$ ratio (~ 10^4) is maintained in order to favor the reaction of interest (R + O_2 → products), and high $[O_2]:[Cl_2]$ is maintained to minimize side reactions (i.e. the ~20-fold excess of O_2 over Cl_2 significantly favors R + O_2 over the chain-chlorination reaction R + Cl_2). High ratios of initial fuel to initial chlorine atom, $[RH]_0:[Cl]_0$, were maintained to ensure a rapid RH + Cl reaction following pseudo-first-order conditions, and suppress secondary reactions of Cl atoms, such as R + Cl and RO_2 + Cl. Under the pseudo-first-order conditions, 2,5-dimethylhexane consumption (measured using time histories of the ^{13}C isotopolog) remained near 10%.

Table 2. Initial number densities and mole fractions for Cl-initiated oxidation experiments at 8 Torr. The number density of He is an average of conditions at 550 K and 650 K.

Species	Number Density (molecules/cm^3)	Mole Fraction
2,5-dimethylhexane	$1.3 \cdot 10^{14}$	0.001
O_2	$2.8 \cdot 10^{16}$	0.219
Cl_2	$1.4 \cdot 10^{14}$	0.001
He	$9.8 \cdot 10^{16}$	0.779

The reacting mixture is continuously sampled from the slow-flow quartz reactor through a 650-μm side orifice into a vacuum chamber (10^{-5} Torr), forming a near-effusive molecular beam. After passing a skimmer, the molecular beam then enters the photoionization region and is crossed with quasi-continuous VUV photons. The cations formed are focused into a 50-kHz pulsed-extraction, orthogonal-acceleration time-of-flight mass spectrometer and detected on a microchannel plate detector. Complete mass spectra were recorded in 20-μs time intervals over a span of 150 ms (20-ms pre-photolysis and 130-ms post-photolysis), producing time-dependent mass spectra. The high mass resolution of the spectrometer ($m/\Delta m$ > 1500) allows distinguishing species with the same nominal mass, yet different elemental composition (e.g., *iso*-butene, C_4H_8, with exact mass 56.06 is differentiable in the mass spectra from propenal, C_3H_4O, of exact mass 56.03).

Scanning the energy of the ionizing synchrotron radiation provides a third dimension to the time-dependent mass spectra, creating a three-dimensional measurement of ion signal as a function of mass-to-charge ratio, time, and photoionization energy: $S(m/z, t, E)$. Ion signals were normalized to the VUV photon flux measured by a calibrated photodiode. Interpretation of all measurements was performed using subtraction of the average pre-photolysis background signal for all *m/z*, yielding difference mass spectra. Osborn et al. [17] and Taatjes et al. [24] provide a more-detailed description of the three-dimensional measurement technique.

Absolute photoionization spectra were measured at 600 K for several species (2,2,5,5-tetramethyltetrahydrofuran, 2,5-dimethylhexane, 2,5-dimethyl-1-hexene/-2-hexene/-3-hexene, and 5-methyl-2-hexene (Supplemental Material)) in accord with the procedure described in [25]. Comparison of the reference spectra of individual species to spectra measured in the oxidation experiments provides both isomer-resolved assignment of different reaction products and quantification of relative concentrations. In cases where experimental photoionization spectra were not available, simulations were conducted using Gaussian09 [26] by integrating the photoelectron spectra obtained using Franck-Condon factor calculations derived from unscaled B3LYP/CBSB7 frequencies and offset using CBS-QB3-calculated adiabatic ionization energies (AIE) [27].

The isomeric composition of the main peaks in the mass spectra was determined using the measured absolute photoionization cross-sections of expected species. Relative yields of the identified species were then defined as the yield of a single species relative to the aggregate yield of conjugate alkene and were quantified using the methodology detailed in the Supplemental Material. In short, for the case where multiple isomers comprise a single mass peak, using absolute photoionization cross-section measurements of the contributing species and correcting for mass discrimination effects [28], ion signals

measured in the oxidation experiments were converted to relative concentration. The absolute photoionization cross-sections, which individually reflect concentration, were then used as basis functions in a non-linear fitting routine to calculate fitting coefficients representing the relative isomeric contributions.

2.2. Computational methods

Isomerization and unimolecular decomposition pathways were calculated for 2,5-dimethyl-1-hexyl automatically using the KinBot code [29] coupled to Gaussian 09 [30] at the M06-2X/6-311++G(d,p) level of theory [31] with an ultrafine grid and tight convergence criteria. The code also determined the lowest energy conformers of the stationary points, and characterized the conformational space by means of one-dimensional dihedral scans. Subsequently, the stationary point energies of the lowest-energy conformers were refined using both CBS-QB3 [27] and unrestricted CCSD(T)-F12a/cc-pVDZ levels of theory; the latter calculations were performed using the Molpro 2012 suite of programs [32, 33]. From the molecular parameters of the stationary points, an RRKM-based master equation model was constructed as implemented in the PAPER code [34] in which the separable 1-D hindered rotor approximation was applied to account for torsional anharmonicities, and using 1-D Eckart barriers to include the effect of tunneling. A simple exponential-down model, $\langle \Delta E_{down} \rangle = 200 \times (T/300\ \mathrm{K})^{0.85}$, was used to account for pressure dependence (collisional energy transfer), and Lennard-Jones parameters $\varepsilon/k_B = 367.5$ K and $\sigma = 6.52$ Å were chosen for the complexes based on the values determined for 2,4-dimethylhexane [35].

3. Results

Difference mass spectra were measured at 550 K and 650 K, integrated over the photon energy range 8.3 – 10.6 eV and post-photolysis times of 30- and 20-ms, respectively (Fig. 3). Both spectra in Fig. 3 were normalized to the peak at *m/z* 113, the main product mass peak. The main peaks in the two spectra are similar, with the exception of *m/z* 42 appearing at 650 K, and correspond to parent ions of products (e.g. *m/z* 112, *m/z* 128) or fragment ions from dissociative ionization (e.g. *m/z* 85, *m/z* 113) from reactions of R with O_2 or from thermal decomposition. The primary products from R + O_2 reactions of 2,5-dimethylhexane (*m/z* 114) are the conjugate alkene (C_8H_{16}, *m/z* 112) and the cyclic ether ($C_8H_{16}O$, *m/z* 128). The *m/z* 113 ion signal is formed by loss of a neutral methyl fragment from cyclic ether species upon ionization and from photodissociation of ROO. The positions of the maxima of other product peaks in the spectra indicate oxygenated species including C_3H_6O (*m/z* 58.042), C_4H_8O (*m/z* 72.057), and C_5H_9O (*m/z* 85.065), and other hydrocarbons including C_3H_6 (*m/z* 42.047), C_4H_8 (*m/z* 56.062), C_5H_{10} (*m/z* 70.078), and C_7H_{14} (*m/z* 98.109). In the ensuing sections, the isomeric identification of species consistent with formation along R + O_2 pathways or decomposition of R is discussed in addition to relevant mechanistic pathways.

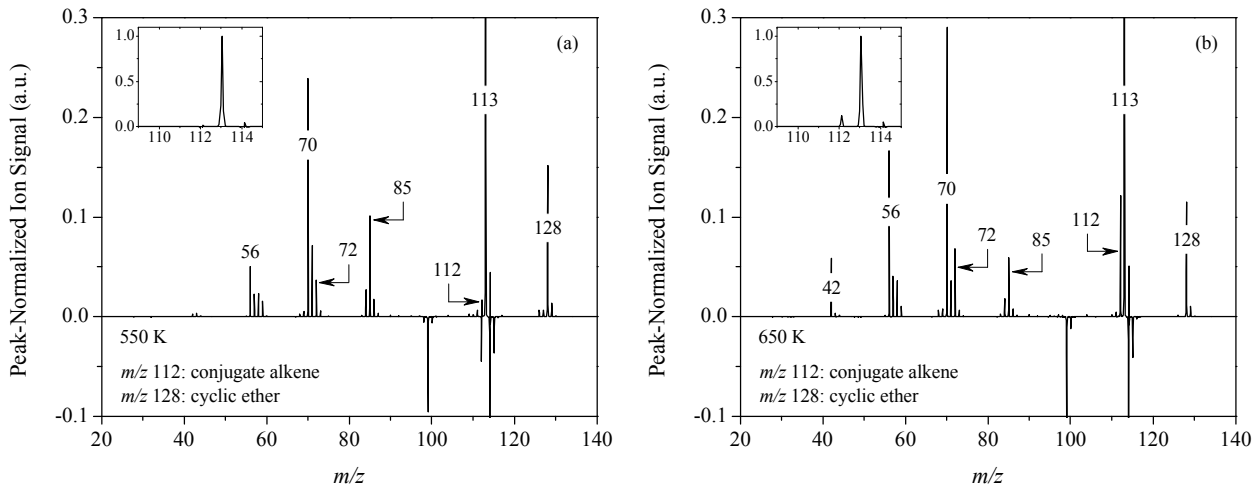

Fig. 3. Difference mass spectra of 2,5-dimethylhexane oxidation (8 Torr) at (a) 550 K and (b) 650 K. *m/z* 113 peaks, formed primarily from fragment ions of cyclic ether species and of ROO radicals, dominate the two spectra (inset). Negative peaks result from depletion of 2,5-dimethylhexane and related fragment ions.

Photon-energy-integrated time histories for mass peaks of primary products are compared in Fig. 4. Due to interference of fragment ion formation from 2,5-dimethylhexane, integration at *m/z* 112 is limited to < 9.8 eV; integration for the other channels spans the entire range (8.3 – 10.6 eV). The time histories in Fig. 4 are normalized to unity at the time limit of the experiment (30-ms for 550 K, 20-ms for 650 K), and are nearly identical at both temperatures, indicating that the *m/z* 56, 58, and 72 timescales are coincident with primary products formed in R + O_2 reactions (*m/z* 112, 128) or from decomposition of R.

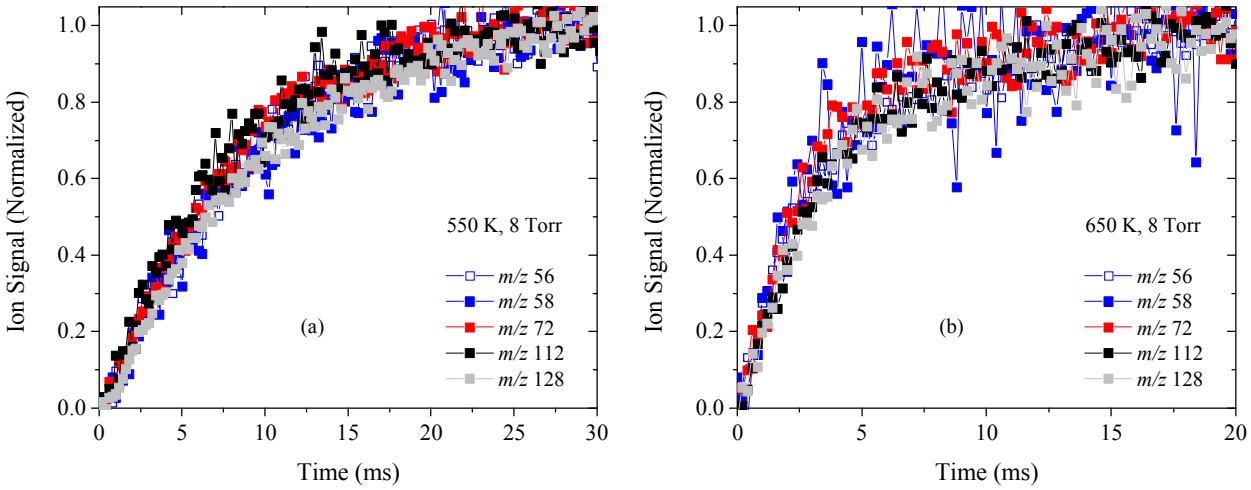

Fig. 4. Normalized time histories of primary product formation at (a) 550 K and (b) 650 K, integrated from 8.3 – 10.6 eV, except *m/z* 112 (8.3 – 9.8 eV) due to fragment ions formed from 2,5-dimethylhexane.

3.1 Product identification and relative yields

Table 3 lists the relative yields at 550 K and 650 K and ionization energies, defined as the photon energy measured at 1% of the peak-normalized ion signal over the energy range 8.3 – 10.6 eV. Uncertainty of ± 50% is assigned to the relative yield calculations, arising mainly from error of ± 20% in the measured absolute photoionization cross-sections, ~ 40% error in the mass discrimination factor, and including a 1σ error calculated in the fitting routine. The peaks at *m/z* 128 and *m/z* 113 are assigned to cyclic ether products and associated fragment ions. Only the absolute photoionization cross-section of 2,2,5,5-tetramethyl-tetrahydrofuran was measured and exhibits a weak partial cross section (0.70 Mb at 10 eV) at the mass of the parent with the remainder fragmenting via loss of neutral CH_3 to $[C_7H_{13}O]^+$ at *m/z* 113. Because other cyclic ether isomers were not obtainable, and a contribution from at least one other cyclic ether isomer is needed to account for the *m/z* 128 signal, it was not possible to determine the relative yield for 2,2,5,5-tetramethyl-tetrahydrofuran. Isomeric compositions of two mass peaks remain unidentified: *m/z* 70 (C_5H_{10}) and *m/z* 85 (C_5H_9O). Time profiles for both *m/z* 70 and *m/z* 85 reflected the formation of

stable species on timescales consistent with primary product formation (cf. Fig. 4) and are most likely caused by dissociative ionization.

Table 3. Nominal relative yields and onset energies of species formed from Cl-initiated oxidation of 2,5-dimethylhexane. Relative yields are defined relative to the sum of conjugate alkene concentration (italicized species), and onset energies correspond to the photon energy measured at 1% of the spectrum normalized to unity over the energy range 8.3 – 10.6 eV. Uncertainty of 50% is assigned to relative yields.

				Relative Yield		
m/z	Chemical Formula	Species	Structure	550 K	650 K	Onset
128	$C_8H_{16}O$	2,2,5,5-tetramethyl-tetrahydrofuran	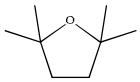	–	–	8.81 eV
112	C_8H_{16}	*2,5-dimethyl-1-hexene*	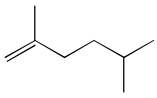	0.50	0.62	8.87 eV
		2,5-dimethyl-2-hexene	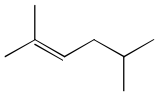	0.33	0.34	8.45 eV
		2,5-dimethyl-3-hexene	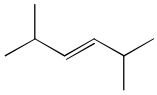	0.17	0.04	8.75 eV
98	C_7H_{14}	5-methyl-2-hexene	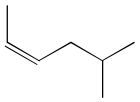	0.00	0.03	8.82 eV
85	C_5H_9O	(unidentified)	–	–	–	9.02 eV
72	C_4H_8O	methylpropanal	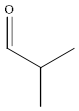	0.42	0.27	9.63 eV
70	C_5H_{10}	(unidentified)	–	–	–	9.02 eV
58	C_3H_6O	acetone		0.12	0.10	9.65 eV
		propanal	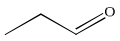	0.06	0.00	9.88 eV
56	C_4H_8	*iso*-butene		0.30	0.40	9.12 eV
42	C_3H_6	propene		0.03	0.17	9.70 eV

3.2 HO_2-loss channels: C_8H_{16} alkene formation

Three C_8H_{16} alkene isomers (*m/z* 112) are associated with direct HO_2-elimination from ROO and with decomposition of QOOH radicals where the radical site is β to the OOH group. In either case, pathways from the primary initial radical lead only to 2,5-dimethylhex-1-ene, while the tertiary radical yields both the hex-1-ene and hex-2-ene structures, and the secondary radical yields both the hex-2-ene and hex-3-ene structures (Fig. 5).

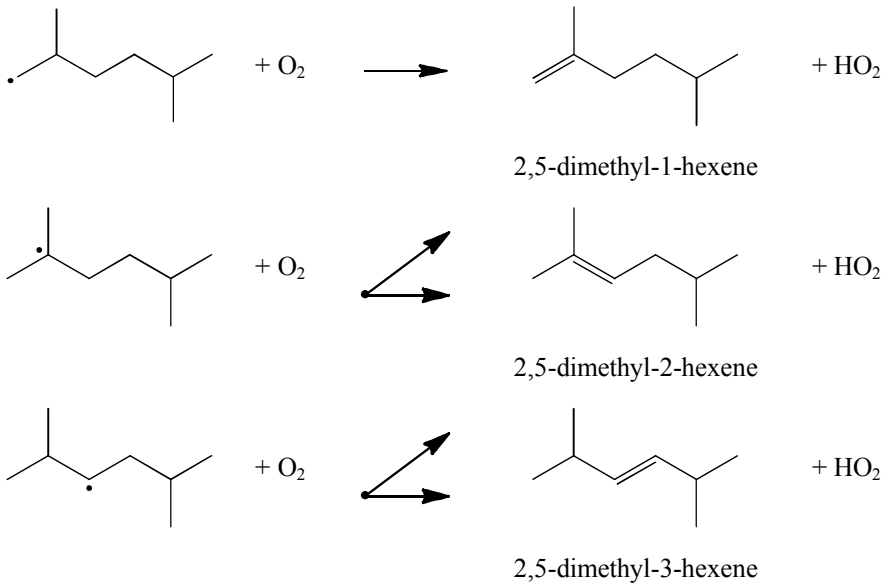

Fig. 5. Conjugate alkene + HO_2 formation in reactions of 2,5-dimethylhexyl radicals with O_2.

Photoionization spectra of the *m/z* 112 product measured in the oxidation experiments were fit to a combination of the absolute photoionization spectra of 2,5-dimethylhex-1-ene, 2,5-dimethylhex-2-ene, and *trans*-2,5-dimethylhex-3-ene (*cis*-2,5-dimethylhex-3-ene was assumed similar) at 550 K and 650 K (Fig. 6). The relative fitting coefficients of the individual species give the isomeric branching ratios. At 550 K, the ratios of the three isomers were: 2,5-dimethylhex-1-ene = 0.50 ± 0.25, 2,5-dimethylhex-2-ene = 0.33 ± 0.16, and 2,5-dimethylhex-3-ene = 0.17 ± 0.08. At 650 K, the nominal relative yield of the 1-hexene isomer increases to 0.62 ± 0.31, and 2,5-dimethylhex-3-ene decreases to 0.04 ± 0.02, with the contribution of the hex-2-ene remaining relatively unchanged: 0.34 ± 0.17. Because the hex-3-ene product is formed only from the reaction of O_2 with the secondary R, the decreasing yield of the hex-3-ene structure with increasing temperature may reflect a diminishing relative role of the secondary 2,5-dimethylhex-3-yl radical to the HO_2-forming channels, and an increase in the rate of conjugate alkene formation from the primary 2,5-dimethylhex-1-yl. However, the uncertainties also create the potential for the branching ratios to remain relatively unchanged from 550 K to 650 K.

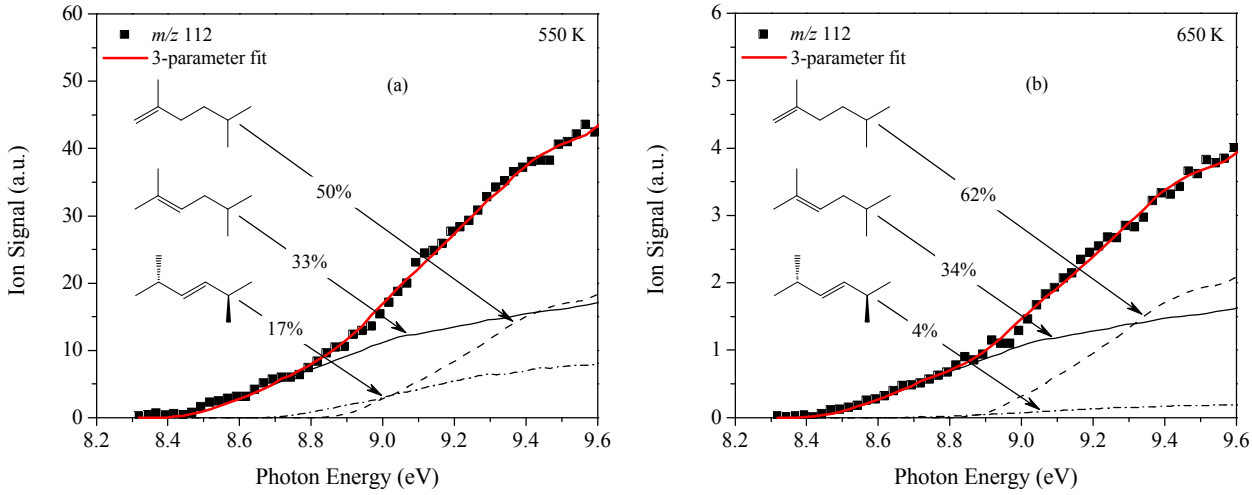

Fig. 6. Photoionization spectra of *m/z* 112 at (a) 550 K and (b) 650 K overlaid with the 3-parameter fit representing the relative isomeric contributions of the three alkenes. The photoionization spectra of the alkenes are scaled in accordance with relative yields (e.g. the cross-section of 2,5-dimethyl-1-hexene is scaled to 50% of the *m/z* 112 signal at 550 K).

3.3 OH formation channels: $C_8H_{16}O$ cyclic ether formation

OH-loss from QOOH radicals of 2,5-dimethylhexane leads to the formation of $C_8H_{16}O$ cyclic ether co-products of nominal *m/z* 128. Ten isomers are possible and, neglecting alkyl radical isomerization reactions, four cyclic ethers are uniquely derived from a specific R (Table 4). Two cyclic ethers are specific to the oxidation of primary alkyl radicals: the 7-membered 2,7-dimethyloxepane and the 4-membered 3-*iso*-pentyl-oxetane. The 3-membered 1,1-diisopropyloxirane arises solely from oxidation of secondary alkyl radicals, and the 5-membered 2,2,5,5-tetramethyl-tetrahydrofuran is formed only from oxidation of the tertiary alkyl radical. The remaining six cyclic ether species can form from multiple initial alkyl radicals (e.g. 2-*iso*-propyl-4-methyl-tetrahydrofuran in Table 4).

In order to identify which cyclic ether species were most energetically favorable from the different 2,5-dimethylhexyl radicals, the generalized theoretical results of Miyoshi [9] on unimolecular reactions of ROO and QOOH were analyzed. Specifically, energy barriers for ROO ⟶ QOOH isomerization and barriers to decomposition of QOOH into cyclic ether + OH, pertinent to 2,5-dimethylhexane oxidation, were extracted from [9] and compared relative to the energies of ROO wells to determine favorable pathways. For the purpose of determining the most favorable cyclic ether formation pathways, barrier heights relative to the ROO well for ROO ⟶ QOOH and for QOOH ⟶ cyclic ether + OH were compiled (Supplemental Material). Barrier heights on the respective R + O_2 surface higher than 10 kcal/mol, relative to the lowest barrier for the given step (isomerization to QOOH or decomposition of QOOH), were regarded as less favorable. At lower temperatures, energy barrier differences of 2 – 3

kcal/mol become exceedingly important, and the results extracted from [9] aided in the identification of active pathways under the experimental conditions utilized herein. Following the 10 kcal/mol criteria, all three alkyl radicals of 2,5-dimethyl hexane contain two energetically favorable cyclic ether pathways.

Table 4. Cyclic ethers, originating 2,5-dimethylhexyl radicals, and ring size of the ROO ⟶ QOOH transition state. Adiabatic ionization energy (AIE) calculations were conducted at the CBS-QB3 level of theory.

Cyclic Ether	Initial R Radical (Ring Size)	AIE	Cyclic Ether	Initial R Radical (Ring Size)	AIE
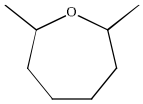	primary R (9)		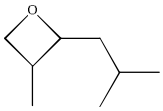	primary R, secondary R (6)	
(a) 2,7-dimethyloxepane		9.15 eV	(f) 2-*iso*-butyl-3-methyl-oxetane		9.21 eV
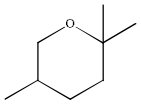	primary R, tertiary R (8)		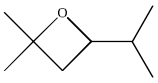	secondary R, tertiary R (6)	
(b) 2,2,5-trimethyl-2-hydropyran		8.95 eV	(g) 2-*iso*-propyl-4,4-dimethyl-oxetane		9.09 eV
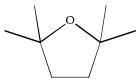	tertiary R (7)		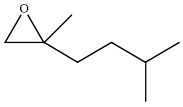	primary R, tertiary R (5)	
(c) 2,2,5,5-tetramethyl-tetrahydrofuran		8.93 eV	(h) 2,2-methyl-*iso*-pentyl-oxirane		9.79 eV
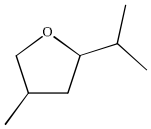	primary R, secondary R (7)		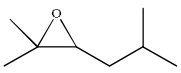	secondary R, tertiary R (5)	
(d) 2-*iso*-propyl-4-methyl-tetrahydrofuran		8.93 eV	(i) 2-*iso*-butyl-3,3-dimethyl-oxirane		9.11 eV
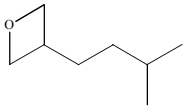	primary R (6)		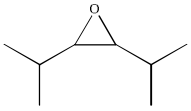	secondary R (5)	
(e) 3-*iso*-pentyl-oxetane		9.58 eV	(j) 2,3-di-*iso*-propyl-oxirane		9.56 eV

For the primary alkyl radical, two low-energy pathways exist and lead to 6-membered and 5-membered cyclic ethers: 2,2,5-trimethyl-2-hydropyran and 2-*iso*-propyl-4-methyl-tetrahydrofuran (species (b) and (d) in Table 4, respectively). The remaining four cyclic ethers potentially formed by the primary radical are likely to be insignificant. The 7-membered cyclic ether in Table 4 (2,7-dimethyloxepane, species (a)) is not considered in [9], and is entropically disfavored due to the 1,8-H-shift from ROO to QOOH, and reliance on abstraction of only primary hydrogen atoms, which exhibit stronger C–H bond strengths compared to secondary or tertiary hydrogen atoms. The isomerization step and QOOH decomposition barrier leading to 3-*iso*-pentyl-oxetane are both high in energy relative to the lowest-lying pathways for the primary alkyl radical. The ROO ⟶ QOOH barrier leading to 2-*iso*-butyl-3-methyl-oxetane is ca. 2 – 3 kcal/mol higher in energy compared to the lowest isomerization barriers, and the barrier leading to the only 3-membered cyclic ether from the primary alkyl is the highest in energy, by 10 – 11 kcal/mol.

For the secondary alkyl radical, the energetically most favorable isomerization barrier to QOOH involves the pathway leading to the 4-membered 2-*iso*-propyl-4,4-dimethyl-oxetane (species (g) in Table 4). The next lowest barriers lead to the 5-membered 2-*iso*-propyl-4-methyl-tetrahydrofuran and the 4-membered 2-*iso*-butyl-3-methyl-oxetane, and are higher by approximately 6 kcal/mol. Similar to the isomerization barriers to QOOH in the primary alkyl, the two 3-membered cyclic ethers derived from the secondary alkyl are highly disfavored. Oxidation of the tertiary alkyl radical strongly favors the formation of 2,2,5,5-tetramethyl-tetrahydrofuran (species (c) in Table 4), with the lowest barrier (by 5 kcal/mol) for ROO ⟶ QOOH and a low-lying QOOH decomposition barrier (ca. 6 kcal/mol). The remaining cyclic ether structures derived from tertiary alkyl radicals are comparatively disfavored.

Summarizing the results extracted from Miyoshi [9] for 2,5-dimethylhexane, four cyclic ethers are the most favorable: 2,2,5-trimethyl-2-hydropyran (primary/tertiary R), 2,2,5,5-tetramethyl-tetrahydrofuran (tertiary R), 2-*iso*-propyl-4-methyl-tetrahydrofuran (primary/secondary R), and 2-*iso*-propyl-4,4-dimethyl-oxetane (secondary/tertiary R). Of the four cyclic ethers and neglecting alkyl radical isomerization, only 2,2,5,5-tetramethyl-tetrahydrofuran is alkyl-radical-specific, yet by comparing the ROO ⟶ QOOH isomerization barriers for the different alkyl radicals, the remaining three cyclic ether may be linked to specific alkyls. Specifically, 2,2,5-trimethyl-2-hydropyran (species (b), Table 4) and 2-*iso*-propyl-4-methyl-tetrahydrofuran (species (d), Table 4) are energetically more favorable from primary-R + O_2, and 2-*iso*-propyl-4,4-dimethyl-oxetane (species g, Table 4) from secondary-R + O_2. Notably, the latter two cyclic ethers potentially contribute to the fragment ion mass peak at *m/z* 85 (cf. Fig. 3) from loss of C_3H_7 upon ionization.

Ignoring entropic effects, the barrier height for the internal abstraction that converts an ROO radical to a QOOH radical is strongly correlated with the energy of the C–H bond that is broken in the isomerization. For a given ring size in the transition-state structure, the two tertiary sites, with 0-K CBS-QB3-calculated C–H bond energy of 95.5 kcal/mol, are the most facile abstraction sites for both the initial H-atom removal step and the internal H-abstraction isomerization ROO ⟶ QOOH. Primary and secondary C–H bond energies of 100.5 and 98.1 kcal/mol were calculated at the CBS-QB3 level of theory, higher than tertiary C–H bond energies by 3 – 5 kcal/mol. Accordingly, O_2 addition to the tertiary R radical, followed by ROO radical isomerization to a tertiary QOOH radical occurs with the lowest barrier [6, 9, 36], making the tertiary-tertiary chemistry leading to 2,2,5,5-tetramethyltetrahydrofuran, energetically favorable in 2,5-dimethylhexane oxidation (Fig. 7).

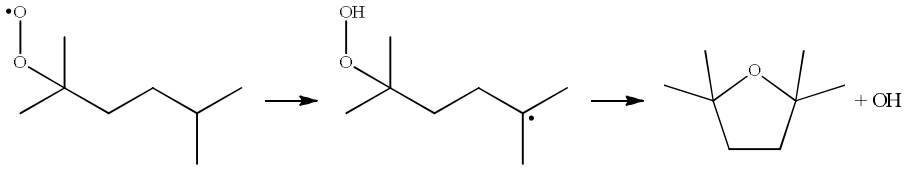

Fig. 7. Decomposition pathway of the tertiary ROO radical forming tertiary QOOH decomposing into 2,2,5,5-tetramethyl-tetrahydrofuran + OH.

Fig. 8 compares the absolute photoionization spectrum of 2,2,5,5-tetramethyltetrahydrofuran, scaled vertically to overlap in the onset region, to the photoionization spectra of *m/z* 128 at 550 K and 650 K. Based on the calculated adiabatic ionization energies in Table 4, only isomers (b), (c), and (d) are expected to contribute to the spectra below 9.0 eV and, as a consequence, isomers arising above 9.0 eV are unlikely species (b) or (d). Qualitatively, the shape of the spectrum of 2,2,5,5-tetramethyltetrahydrofuran closely reflects the shape of the cyclic ether spectrum at both temperatures. Despite the single-species comparison, the highly similar spectra in Figs. 8a and 8b suggest the 2,2,5,5-tetramethyltetrahydrofuran + OH chain-propagation channel is significant in the initial oxidation steps of 2,5-dimethylhexane, particularly given the weak cross-section of the cyclic ether (0.70 Mb at 10 eV). However, at energies above ~ 9.0 eV the *m/z* 128 product spectrum is not solely composed of 2,2,5,5-tetramethyl-tetrahydrofuran, suggesting the presence of at least one other cyclic ether isomer.

One subtle, yet important distinction between the results in Fig. 8 is the larger contribution of 2,2,5,5-tetramethyl-tetrahydrofuran to the aggregate cyclic ether yield at 650 K relative to 550 K, despite being derived solely from tertiary alkyl radicals. In general, the preference for the pathway with the lowest energetic barrier decreases with increasing temperature (i.e. bond energy difference become less hindering on ROO ⟶ QOOH isomerization), which implies in the present case that the contribution of the other, energetically less-favored cyclic ethers increases at the expense of the likely most-favored

cyclic ether, 2,2,5,5-tetramethyltetrahydrofuran. Comparison of the spectra in Fig. 8 reflects the opposite trend, indicating a positive temperature dependence and an increase in the relative contribution to the cyclic ether channel from 2,2,5,5-tetramethyltetrahydrofuran which initiates only from tertiary alkyl radicals (Fig. 7). The JSR results in Sarathy et al. [7] reported a similar temperature dependence, with peak 2,2,5,5-tetramethyl-tetrahydrofuran yield occurring near 650 K. The prominence of the pathway that arises from the tertiary initial alkyl radical in Fig. 7 is further underscored by the results of the SAR calculations, which predict tertiary alkyl radicals comprise the smallest amount of the initial alkyl radical pool in the present Cl-initiated oxidation experiments (cf. Table 1). It is therefore likely that additional mechanisms involving isomerization to tertiary alkyl radicals are important to 2,5-dimethylhexane oxidation under the conditions of the experiments herein.

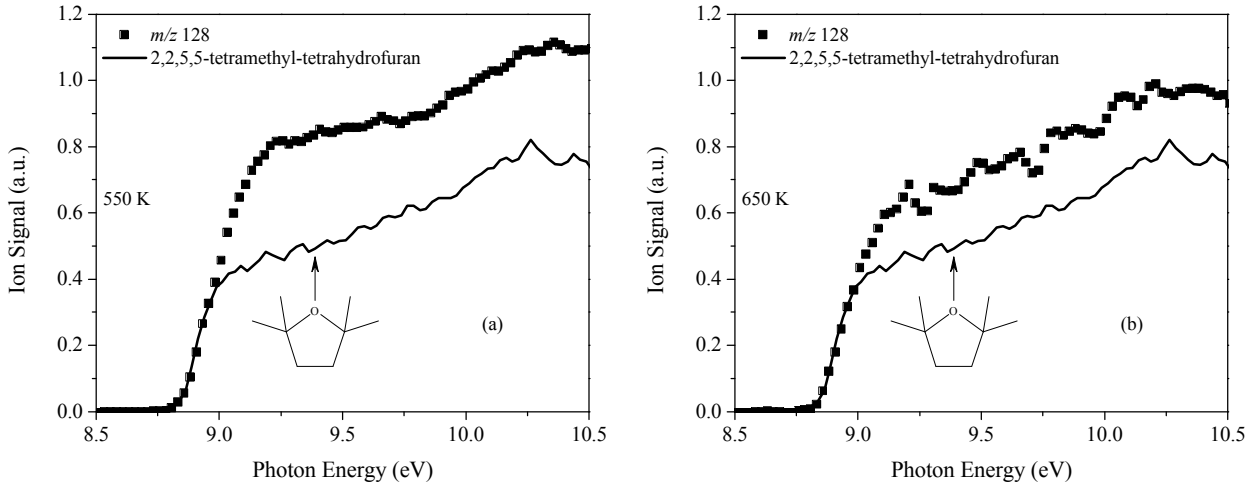

Fig. 8. Photoionization spectra of *m/z* 128 (cyclic ether) at (a) 550 K and (b) 650 K overlaid with the absolute photoionization spectrum of 2,2,5,5-tetramethyl-tetrahydrofuran scaled to align with the slope at the onset energy (8.8 eV) of the *m/z* 128 signal. The non-overlapping signals at photon energies above 9.0 eV indicate isomeric contribution from other cyclic ether species. At 650 K, a larger contribution to the cyclic ether channel from 2,2,5,5-tetramethyl-tetrahydrofuran is observed (inferred from the smaller quantitative difference relative to 550 K).

3.4 Role of primary alkyl isomerization in the formation of 2,2,5,5-tetramethyl-tetrahydrofuran

The increase in temperature from 550 to 650 K in the experiments gives rise to changes in product yields from unimolecular dissociation or from isomerization of the initial alkyl radicals. The mass spectra at 650 K indicated a higher yields of species with *m/z* consistent with alkenes from *β*-scission products of the initial alkyl radicals compared to 550K (cf. Fig. 3, Table 3). The SAR calculations predict that the primary radical is the major alkyl isomer from Cl atom reaction with 2,5-dimethylhexane, remaining the same fraction at both 550 K and 650 K (cf. Table 1). In order to determine the most-favorable consumption pathway of the primary R, an analysis of the different bimolecular reactions, isomerization, and decomposition pathways, including scission of C–H and C–C bonds, is required. If the rate of primary alkyl radical isomerization via 1,5-H-atom shift to the tertiary alkyl radical is sufficiently high, the initially formed primary alkyl radicals could indirectly contribute to 2,2,5,5-tetramethyl-tetrahydrofuran formation. For the contribution to be significant, R isomerization rates via 1,5-H-atom shifting must compete with the rates of other isomerization pathways, O_2-addition, and *β*-scission.

The zero-point-energy corrected barrier heights for isomerization and *β*-scission pathways, calculated for the primary alkyl radical (2,5-dimethylhex-1-yl) at the CCSD(T)-F12a/cc-pVDZ//M06-2X/6-311++G(d,p) level of theory, are compared in Fig. 9. Due to the symmetry of 2,5-dimethylhex-1-yl, isomerization via 1,2- and 1,5-H atom shift , and 1,3- and 1,4-H atom shift reactions lead to the same product radicals: tertiary 2,5-dimethylhex-2-yl and secondary 2,5-dimethylhex-3-yl, respectively. Three *β*-scission channels exist for 2,5-dimethylhex-1-yl, producing (i) *iso*-pentyl + propene, (ii) 5-methyl-1-hexene + methyl, or (iii) 2,5-dimethyl-1-hexene + H. However, the energetically most-favorable channel is the 1,5-H-atom shift via the 6-member ring transition state leading to the tertiary alkyl radical.

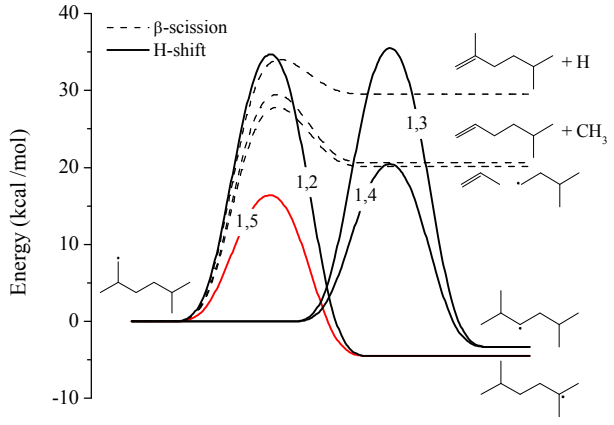

Fig. 9. ZPE-corrected 0-K barrier heights (kcal/mol) at the CCSD(T)-F12a/cc-pVDZ//M06-2X/6-311++G(d,p) level of theory for 2,5-dimethylhex-1-yl decomposition and isomerization pathways. Isomerization via 1,5-H-shift is energetically favored over other isomerization pathways and *β*-scission pathways.

Table 5 lists the unimolecular rate coefficients for the decomposition pathways of 2,5-dimethyl-1-hexyl at 550 and 650 K at 8 Torr, obtained from master-equation calculations using both the CBS-QB3 and CCSD(T)-F12a/cc-pVDZ//M06-2X/6-311++G(d,p) energies. At both temperatures, the highest unimolecular reaction rate of the primary alkyl is the 1,5-H-atom shift forming the tertiary alkyl radical. The differences between the results of the two calculations are in accord with the differences in the barrier heights, listed in Table 5. Note that besides the uncertainties in the barrier heights, the separable 1-D hindered rotor is also a source of uncertainty in the calculated rate coefficients, but not to an extent that alters the following conclusions.

Assuming $k_{(R+O_2)} \sim 10^{-12}$ cm^3 molecule^{-1} s^{-1}, the pseudo-first-order rate coefficient for the R + O_2 reaction is $k' = k_{(R+O_2)}[O_2] \sim 2.8 \cdot 10^4$ s^{-1}. From the trend evident in Table 5, the isomerization rate of 2,5-dimethylhex-1-yl to 2,5-dimethylhex-3-yl increases with temperature and is predicted to be competitive with the O_2 addition rate of at both temperatures. The temperature dependence of the R + O_2 reaction rate coefficient is likely to be minor, therefore at higher temperatures the importance of primary alkyl radical isomerization increases, evidenced by the increased relative yield for the cyclic ether product from the tertiary R + O_2 channel (i.e. 2,2,5,5-tetramethyl-tetrahydrofuran, cf. Fig. 8) in agreement with the experimental observation (cf. Fig. 8).

Table 5. ZPE-corrected barrier heights and calculated rate coefficients at the CBS-QB3 and CCSD(T)-F12a/cc-pVDZ levels of theory for the isomerization and decomposition of 2,5-dimethyl-1-hexyl at 550 and 650 K and 8 Torr. The pairs of numbers for the first two channels reflect the 3- and 6-, and the 4- and 5-member ring barrier heights, respectively.

		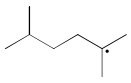	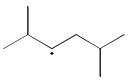	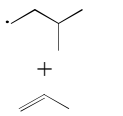	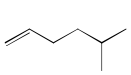	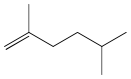
				+	+	+
					CH_3	H
ZPE-corrected barrier height (kcal mol^{-1})	CBS-QB3	36.1/16.2	37.0/20.8	27.1	28.9	33.4
	CCSD(T)-F12a	36.3/17.2	37.1/21.4	28.4	30.1	34.5
$k_{550\,K}$ (s^{-1})	CBS-QB3	**$2.8 \cdot 10^4$**	$2.7 \cdot 10^3$	$1.1 \cdot 10^3$	41.0	0.07
	CCSD(T)-F12a	**$7.9 \cdot 10^3$**	$1.3 \cdot 10^3$	$4.4 \cdot 10^2$	17.0	0.05
$k_{650\,K}$ (s^{-1})	CBS-QB3	**$1.3 \cdot 10^5$**	$2.2 \cdot 10^4$	$2.3 \cdot 10^4$	$1.0 \cdot 10^3$	3.0
	CCSD(T)-F12a	**$4.9 \cdot 10^4$**	$1.3 \cdot 10^4$	$1.2 \cdot 10^4$	$5.8 \cdot 10^2$	3.0

The computational results are corroborated by the experimental identification of species consistent with β-scission of primary and secondary alkyls which lead to radical-specific alkenes. One of the two β-scission pathways of primary R leads to 5-methyl-1-hexene (*m/z* 98), and one of the two β-scission pathways of secondary R leads to 5-methyl-2-hexene (*m/z* 98). Figure 10 depicts the integrated *m/z* 98 product signal at 650 K compared to a scaled photoionization spectrum of 5-methyl-2-hexene. No evidence of a second *m/z* 98 species (i.e. 5-methyl-1-hexene) is apparent since the 5-methyl-2-hexene spectrum completely overlaps the observed *m/z* 98 product signal.

Adiabatic ionization energies and photoionization spectra of the two alkenes were calculated from Franck-Condon factor simulations (Fig. 10). The CBS-QB3-calculated AIE of 5-methyl-1-hexene of 9.34 eV lies above the experimental onset of 8.8 eV for the m/z 98 signal, and the shape of the computed 5-methyl-1-hexene photoionization spectrum is also in disagreement with the *m/z* 98 product signal. In contrast, both the experimental and simulated spectra of 5-methyl-2-hexene overlap the *m/z* 98 spectrum. The agreement of the measured and calculated photoionization spectra in Fig. 10 indicates that the *m/z* 98 signal originates predominantly from β-scission of the secondary alkyl which yields 5-methyl-2-hexene. Based on the results given in Table 5, the primary alkyl preferentially isomerizes to the tertiary alkyl or undergoes an addition reaction with O_2 rather than β-scission. Although QOOH-mediated pathways to *m/z* 98 alkenes exist for the primary alkyl radical, lower-energy pathways (i.e. cyclic ether, HO_2-elimination pathways) are likely to be favored.

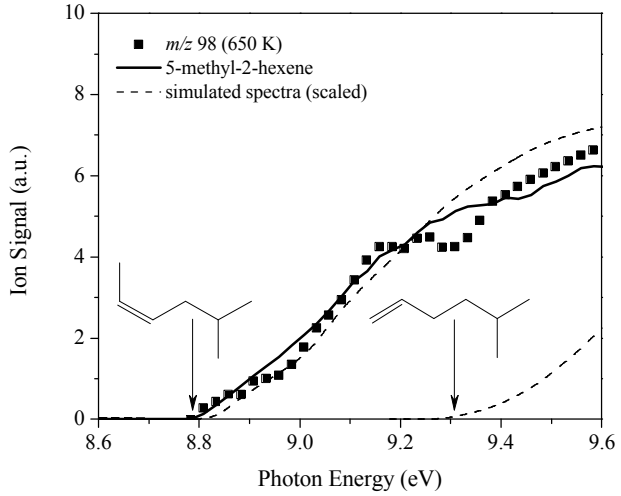

Fig. 10. Comparison of photoionization product spectra of *m/z* 98 at 650 K with a scaled photoionization spectrum of 5-methyl-2-hexene and Franck-Condon simulations for 5-methyl-2-hexene and 5-methyl-1-hexene. The identification of 5-methyl-2-hexene indicates β-scission reactions of the secondary initial alkyl radical. 5-methyl-1-hexene, derived from primary alkyl radicals, is not observed in the *m/z* 98 product spectra. Arrows indicate the CBS-QB3-calculated adiabatic ionization energies for the corresponding alkene.

3.5 QOOH *β*-scission channels: carbonyl + alkene + OH

Chain-propagation reactions involving C–C *β*-scission of QOOH radicals lead to carbonyl + alkene + OH (cf. Fig. 1), and two *m/z* peaks consistent with carbonyl species were measured: *m/z* 58 (C_3H_6O) and *m/z* 72 (C_4H_8O). Photoionization spectra integrated for *m/z* 58 at 550 K and 650 K correlate primarily with acetone, yet at 550 K for photon energies > 10.2 eV, other C_3H_6O isomers appear (Fig. 11a). Minor signal from unknown species is observable at both temperatures from ~ 9.30 eV up to the onset energy of acetone at 9.65 eV. Near 9.8 eV, the acetone spectrum deviates from the *m/z* 58 trend. Inclusion of the photoionization spectrum of propanal compares favorably with the *m/z* 58 trend above 9.8 eV, and the calculated 2-parameter fit reflects a ratio of 60:40 for acetone:propanal. Propanal potentially arises from *β*-scission of the primary *δ*-QOOH species, leading to an oxygenated bi-radical + *iso*-pentene + OH. A 1,2-H shift reaction of the bi-radical then leads to propanal. Other possible contributors to the *m/z* 58 ion signal may include fragment ions of cyclic ether species, including 2,2,5,5-tetramethyltetrahydrofuran or other, cyclic ethers (after loss of a C_5H_{10} fragment) given the correspondence of exact mass measurements to C_3H_6O (*m/z* 58.042). However, at 650 K the *m/z* 58 signal is reproduced completely by the acetone cross-section, and no fragment ion signal is apparent (Fig. 11b). Therefore, the *m/z* 58 spectrum at 550 K most likely includes contribution from propanal. Photoionization spectra integrated for *m/z* 72 at 550 K and 650 K agree with the photoionization spectrum of methylpropanal [19] at both 550 K and 650 K (Fig. 12). At 550 K, a weak, unknown signal with an onset energy of 9.1 eV indicates contribution from an unidentified C_4H_8O isomer other than methylpropanal (Fig. 12a). Similar to acetone and the *m/z* 58 spectrum, at 650 K *m/z* 72 is reproduced solely by methylpropanal, and no fragment ion interference is apparent.

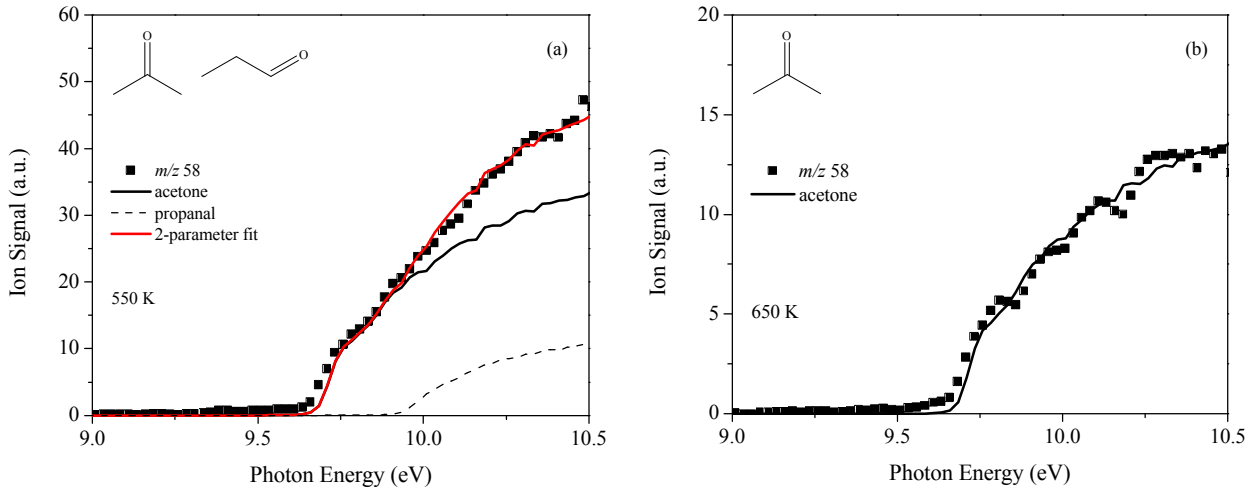

Fig. 11. Photoionization spectra of *m/z* 58 at (a) 550 K and (b) 650 K, scaled to the photoionization cross-section of acetone [25] and propanal [19]. Ion signal with an onset near 9.35 eV is present at photon energies below 9.6 eV, potentially resulting from fragment ions of cyclic ethers.

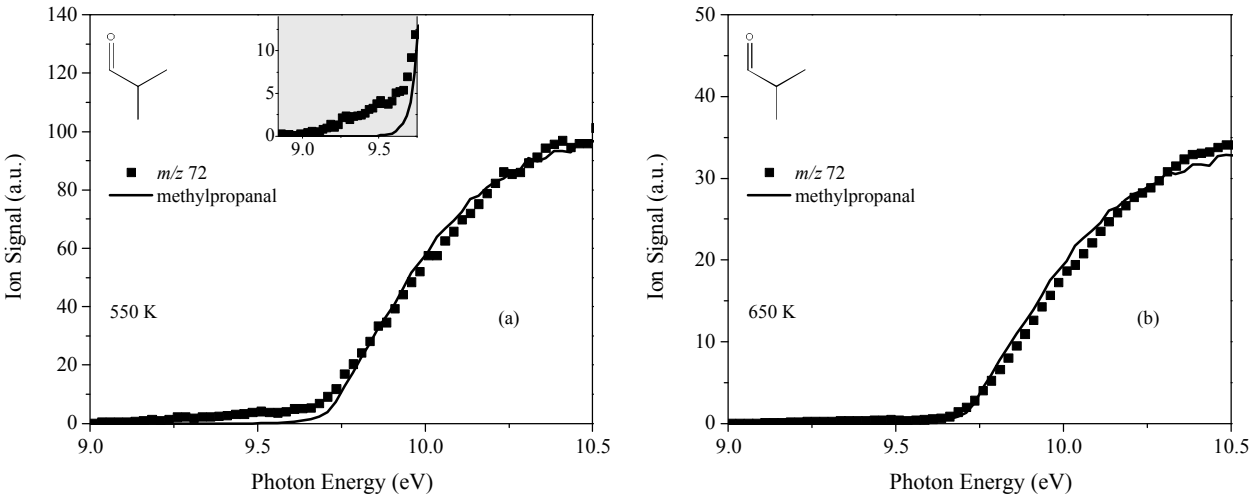

Fig. 12. Integrated ion signal of *m/z* 72 at (a) 550 K and (b) 650 K compared against the photoionization cross-section of methylpropanal [19]. Ion signal from unidentified species of composition C_4H_8O is observed at 550 K from 9.1 eV – 9.6 eV (inset, Fig. 12a).

Timescales for formation of acetone and methylpropanal are consistent with primary oxidation products (cf. Fig. 4), suggesting a mechanism leading to both carbonyl species which involves QOOH radicals. Formation pathways for acetone and methylpropanal arise from β-scission of unique QOOH isomers, derived from the tertiary and secondary initial alkyl radicals, respectively. Decomposition of the tertiary β-QOOH radical via C-C β–scission leads to acetone + *iso*-pentene + OH (Fig. 13), and a β–scission of pathway of the secondary γ-QOOH leads to methylpropanal + *iso*-butene + OH (Fig. 14). Moreover, the alkene co-products were formed on identical timescales, lending further support for acetone and methylpropanal formation coming from QOOH. Although the formation timescales indicate that the two carbonyl species stem from QOOH radicals, secondary reactions leading to acetone and methylpropanal might contribute to some extent, principally bimolecular reactions R + RO_2, RO_2 + RO_2, or reactions of OH with conjugate alkenes (isomers of 2,5-dimethylhexene) via the Waddington mechanism [37, 38], i.e. OH + alkene ⟶ carbonyl + carbonyl + OH. Addition of OH to 2,5-dimethyl-2-hexene leads to acetone + 4-methylpentanal + OH, and addition of OH to 2,5-dimethyl-3-hexene to methylpropanal + OH. Ion signal at *m/z* 100, corresponding to 4-methylpentanal, is not present in the mass spectra at either 550 K or 650 K, indicating that acetone formation is not due to OH + 2,5-dimethyl-2-hexene. The Waddington mechanism leading to methylpropanal, however, cannot be excluded.

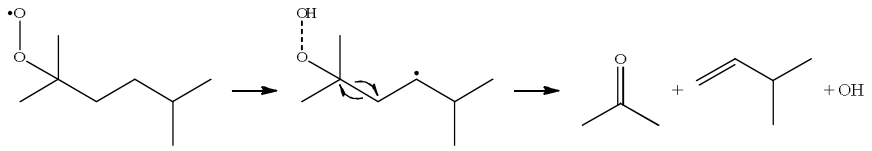

Fig. 13. Acetone formation from the tertiary ROO radical (2,5-dimethyl-2-hexyl) forming secondary γ-QOOH leading to acetone + *iso*-pentene + OH from C–C bond scission.

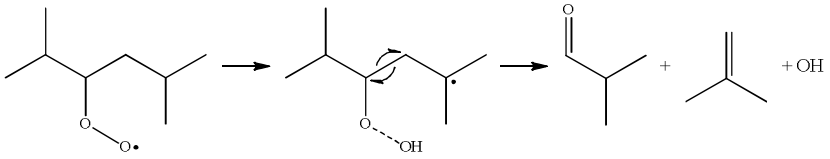

Fig. 14. Methylpropanal formation from the secondary ROO radical (2,5-dimethyl-3-hexyl) forming tertiary γ-QOOH leading to methylpropanal + *iso*-butene + OH from C–C bond scission.

Due to the inability to determine the relative yield of all the cyclic ether isomers, it is not possible to compare the major tendencies of the initial radicals or QOOH radicals. However, the relative yields of acetone and methylpropanal (cf. Table 3) potentially indicate that the formation channels to carbonyls are important in 2,5-dimethylhexane oxidation. Taking the channels as primary oxidation mechanisms, C–C β–scission of QOOH radicals leading to acetone and methylpropanal potentially involve favorable energetic barriers. Accordingly, potential energy surface calculations for the reactions of the three 2,5-dimethylhexyl radicals with O_2 could address the tendencies of QOOH radicals to form cyclic ethers or undergo β-scission reactions leading to carbonyls, in addition to confirming the cyclic ether trends predicted using the results of Miyoshi [9].

4 Component-centered approach towards low-temperature biofuel combustion

Complex molecular structures of bio-derived fuels necessitate a systematic approach to determine the impact of specific functional groups on fuel oxidation pathways and, more broadly, to assess the practical viability of these compounds in fuel-flexible engines. The results of the present work contribute to a component-centered approach towards the study of low-temperature oxidation trends of structurally complex fuels (e.g. bisabolane, Fig. 15a) via characterization of smaller representative molecules. In the case of bisabolane, a microbially derived sesquiterpenoid fuel produced by fermentation [2], the effects of specific structural features can be investigated using separate studies on limonane (covering ring/side-chain interactions) and methylcyclohexane and 2,5-dimethylhexane (covering ring and branched side-chain parts independently).

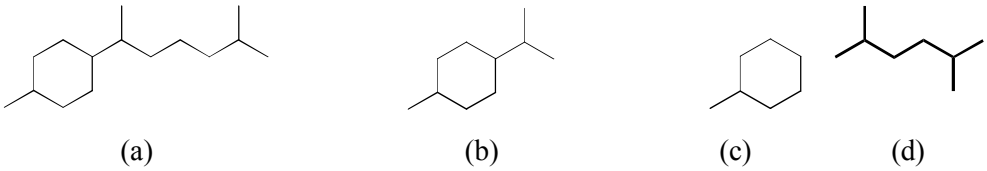

Fig. 15. Molecular structures of (a) bisabolane ($C_{15}H_{30}$) and sub-structures (b) limonane, (c) methylcyclohexane, and (d) 2,5-dimethylhexane.

The influence of close-proximity tertiary alkyl radicals on low-temperature chain-propagation trends and an important role of primary alkyl radicals were uncovered in the present work by studying 2,5-dimethylhexane. The results bring to light the implications of primary alkyl radical isomerization being favored over reaction with O_2. Similar radical isomerization may occur in bisabolane or limonane, in which case side-chain chemistry at low temperature may be dominated by pathways stemming from tertiary radicals with increasing temperature. However, given the high concentrations of O_2 present in practical combustion systems, the degree to which the H-atom shift reactions observed herein impact autoignition warrants continued exploration.

Conclusion

Multiplexed photoionization mass spectrometry experiments and theoretical kinetics calculations were conducted on the initial steps of 2,5-dimethylhexane oxidation to identify relevant ROO-related product formation pathways. The analysis focused on the formation of primary products: conjugate alkene, cyclic ether, and carbonyls from QOOH β-scission. Temperature-dependent branching ratios for the HO_2 + conjugate alkene channels were quantified at 550 K and 650 K. While ten different cyclic ether species are possible in 2,5-dimethylhexane oxidation, the experiments herein indicate that 2,2,5,5-tetramethyl-tetrahydrofuran, formed by reaction of the tertiary radical 2,5-dimethylhex-2-yl with O_2, is significant and exhibits a positive temperature dependence from 550 K to 650 K with respect to aggregate cyclic ether yield. The calculated rate coefficients for unimolecular reactions of the primary radical 2,5-dimethylhex-1-yl reveal that the increase in 2,2,5,5-tetramethyl-tetrahydrofuran yield with temperature is likely caused by facile primary-tertiary alkyl radical isomerization prior to O_2-addition, a process that is also favored over primary alkyl β-scission at low temperature. Three carbonyl species consistent with QOOH decomposition by β-scission were identified experimentally: acetone, propanal, and methylpropanal. The correspondence of the time profiles with cyclic ether and conjugate alkene products indicates that the carbonyl species potentially stem from QOOH radicals that may be important contributors to low-temperature chain-propagation of 2,5-dimethylhexane.

Studying the low-temperature autoignition chemistry of complex next-generation biofuels, with molecular structures combining several features common to conventional petroleum-based fuels, benefits from the component-centered approach outlined herein. The approach entails separate, targeted studies conducted on molecules with specific structural features which complement a larger, more-complex fuel of interest. Studying 2,5-dimethylhexane oxidation serves as a first step towards decoding more complex systems such as bisabolane, a microbially-derived sesquiterpenoid biofuel with both cyclic and branched alkane features. Taking such a component-centered approach contributes to gaining broader predictability of the autoignition and combustion characteristics of structurally complex biofuels.

Acknowledgements

The authors acknowledge financial support from the Department of Energy under Award Number DE-PI0000012, supported by the U.S-China Clean Energy Research Center (CERC) Clean Vehicle Consortium. JZ, OW, LS, AMS, JDS, DLO, and the development and maintenance of the MPIMS kinetics machine are supported by the U.S. Department of Energy, Office of Science, Office of Basic Energy Sciences. The research conducted used resources of the Advanced Light Source, which is a DOE Office of Science User Facility at Lawrence Berkeley National Laboratory under Contract DE-AC02-05CH11231. Sandia is a multi-program laboratory operated by Sandia Corporation, a Lockheed Martin Company, for the National Nuclear Security Administration under contract DE-AC04-94-AL85000.

References

[1] W. J. Pitz, N. P. Cernansky, F. L. Dryer, F. N. Egolfopoulos, J. T. Farrell, D. G. Friend, H. Pitsch, *SAE Technical Paper 2007-01-0175* 10.4271/2007-01-0175 (2007)
[2] P. P. Peralta-Yahya, F. Zhang, S. B. del Cardayre, J. D. Keasling, *Nature* **488** (7411) (2012) 320-328.
[3] T. J. Bruno, E. Baibourine, *Energy & Fuels* **25** (4) (2011) 1847-1858.
[4] C. K. Westbrook, *Proc. Combust. Inst.* **28** (2000) 1563-1577.
[5] C. Morley, *Combustion Science and Technology* **55** (4-6) (1987) 115-123.
[6] J. Pfaendtner, X. Yu, L. J. Broadbelt, *The Journal of Physical Chemistry A* **110** (37) (2006) 10863-10871.
[7] S. M. Sarathy, T. Javed, F. Karsenty, A. Heufer, W. Wang, S. Park, A. Elwardany, A. Farooq, C. K. Westbrook, W. J. Pitz, M. A. Oehlschlaeger, G. Dayma, H. J. Curran, P. Dagaut, *Combust. Flame* **161** (6) (2014) 1444-1459.
[8] R. R. Baldwin, M. W. M. Hisham, R. W. Walker, *Journal of the Chemical Society, Faraday Transactions 1: Physical Chemistry in Condensed Phases* **78** (5) (1982) 1615-1627.
[9] A. Miyoshi, *The Journal of Physical Chemistry A* **115** (15) (2011) 3301-3325.
[10] S. M. Villano, L. K. Huynh, H.-H. Carstensen, A. M. Dean, *The Journal of Physical Chemistry A* **115** (46) (2011) 13425-13442.
[11] S. M. Villano, L. K. Huynh, H.-H. Carstensen, A. M. Dean, *The Journal of Physical Chemistry A* **116** (21) (2012) 5068-5089.
[12] J. Zádor, R. X. Fernandes, C. A. Taatjes, *Prog. Energy Comb. Sci.* **37** (4) (2011) 371-421.
[13] C. A. Taatjes, *The Journal of Physical Chemistry A* **110** (13) (2006) 4299-4312.
[14] F. Battin-Leclerc, *Prog. Energy Comb. Sci.* **34** (4) (2008) 440-498.
[15] P. A. Heimann, M. Koike, C. W. Hsu, D. Blank, X. M. Yang, A. G. Suits, Y. T. Lee, M. Evans, C. Y. Ng, C. Flaim, H. A. Padmore, *Review of Scientific Instruments* **68** (5) (1997) 1945-1951.
[16] S. R. Leone, M. Ahmed, K. R. Wilson, *Phys Chem Chem Phys* **12** (25) (2010) 6564-6578.
[17] D. L. Osborn, P. Zou, H. Johnsen, C. C. Hayden, C. A. Taatjes, V. D. Knyazev, S. W. North, D. S. Peterka, M. Ahmed, S. R. Leone, *Rev. Sci. Inst.* **79** (10) (2008) 104103-10.
[18] J. D. Savee, O. Welz, C. A. Taatjes, D. L. Osborn, *Phys Chem Chem Phys* **14** (30) (2012) 10410-10423.
[19] O. Welz, J. D. Savee, A. J. Eskola, L. Sheps, D. L. Osborn, C. A. Taatjes, *Proc. Combust. Inst.* **34** (1) (2013) 493-500.
[20] R. Atkinson, *Int. J. Chem. Kin.* **19** (9) (1987) 799-828.
[21] R. S. Lewis, S. P. Sander, S. Wagner, R. T. Watson, *The Journal of Physical Chemistry* **84** (16) (1980) 2009-2015.
[22] R. Atkinson, D. L. Baulch, R. A. Cox, J. N. Crowley, R. F. Hampson, R. G. Hynes, M. E. Jenkin, M. J. Rossi, J. Troe, I. Subcommittee, *Atmos. Chem. Phys.* **6** (11) (2006) 3625-4055.
[23] J. H. Knox, R. L. Nelson, *Transactions of the Faraday Society* **55** (0) (1959) 937-946.
[24] C. A. Taatjes, N. Hansen, D. L. Osborn, K. Kohse-Hoinghaus, T. A. Cool, P. R. Westmoreland, *Phys Chem Chem Phys* **10** (1) (2008) 20-34.
[25] O. Welz, J. Zador, J. D. Savee, M. Y. Ng, G. Meloni, R. X. Fernandes, L. Sheps, B. A. Simmons, T. S. Lee, D. L. Osborn, C. A. Taatjes, *Phys Chem Chem Phys* **14** (9) (2012) 3112-3127.
[26] M. J. Frisch, G. W. Trucks, H. B. Schlegel, G. E. Scuseria, M. A. Robb, J. R. Cheeseman, G. Scalmani, V. Barone, B. Mennucci, G. A. Petersson, H. Nakatsuji, M. Caricato, X. Li, H. P. Hratchian, A. F. Izmaylov, J. Bloino, G. Zheng, J. L. Sonnenberg, M. Hada, M. Ehara, K. Toyota, R. Fukuda, J. Hasegawa, M. Ishida, T. Nakajima, Y. Honda, O. Kitao, H. Nakai, T. Vreven, J. Montgomery, J. A., J. E. Peralta, F. Ogliaro, M. Bearpark, J. J. Heyd, E. Brothers, K. N. Kudin, V. N. Staroverov, R. Kobayashi, J. Normand, K. Raghavachari, A. Rendell, J. C. Burant, S. S. Iyengar, J. Tomasi, M. Cossi, N. Rega, J. M. Millam, M. Klene, J. E. Knox, J. B. Cross, V. Bakken, C. Adamo, J. Jaramillo, R. Gomperts, R. E. Stratmann, O. Yazyev, A. J. Austin, R. Cammi, C. Pomelli, J. W. Ochterski, R. L. Martin, K. Morokuma, V. G. Zakrzewski, G. A. Voth, P. Salvador, J. J. Dannenberg, S. Dapprich, A. D. Daniels, Ö. Farkas, J. B.

Foresman, J. V. Ortiz, J. Cioslowski, D. J. Fox, (Gaussian 09, Revision A.1 Gaussian, Inc., Wallingford CT, 2009)
[27] J. A. Montgomery, M. J. Frisch, J. W. Ochterski, G. A. Petersson, *The Journal of Chemical Physics* **110** (6) (1999) 2822-2827.
[28] J. D. Savee, S. Soorkia, O. Welz, T. M. Selby, C. A. Taatjes, D. L. Osborn, *The Journal of Chemical Physics* **136** (13) (2012) -.
[29] J. Zádor;, N. H. Najm;, in: Sandia National Laboratories: 2012.
[30] M. J. Frisch, G. W. Trucks, H. B. Schlegel, G. E. Scuseria, M. A. Robb, J. R. Cheeseman, G. Scalmani, V. Barone, B. Mennucci, G. A. Petersson, H. Nakatsuji, M. Caricato, X. Li, H. P. Hratchian, A. F. Izmaylov, J. Bloino, G. Zheng, J. L. Sonnenberg, M. Hada, M. Ehara, K. Toyota, R. Fukuda, J. Hasegawa, M. Ishida, T. Nakajima, Y. Honda, O. Kitao, H. Nakai, T. Vreven, J. Montgomery, J. A., J. E. Peralta, F. Ogliaro, M. Bearpark, J. J. Heyd, E. Brothers, K. N. Kudin, V. N. Staroverov, R. Kobayashi, J. Normand, K. Raghavachari, A. Rendell, J. C. Burant, S. S. Iyengar, J. Tomasi, M. Cossi, N. Rega, N. J. Millam, M. Klene, J. E. Knox, J. B. Cross, V. Bakken, C. Adamo, J. Jaramillo, R. Gomperts, R. E. Stratmann, O. Yazyev, A. J. Austin, R. Cammi, C. Pomelli, J. W. Ochterski, R. L. Martin, K. Morokuma, V. G. Zakrzewski, G. A. Voth, P. Salvador, J. J. Dannenberg, S. Dapprich, A. D. Daniels, Ö. Farkas, J. B. Foresman, J. V. Ortiz, J. Cioslowski, D. J. Fox, in: Gaussian, Inc.: Wallingford CT, 2009.
[31] Y. Zhao, D. Truhlar, *Theor Chem Account* **120** (1-3) (2008) 215-241.
[32] H. J. Werner, P. J. Knowles, G. Knizia, F. R. Manby, M. Schutz, *Wiley Interdiscip. Rev.-Comput. Mol. Sci.* **2** (2) (2012) 242-253.
[33] H.-J. Werner, P. J. Knowles, G. Knizia, F. R. Manby, M. Schütz, M. Celani, T. Korona, R. Lindh, A. Mitrushenkov, G. Rauhut, K. R. Shamasundar, T. B. Adler, R. D. Amos, A. Bernhardsson, A. Berning, D. L. Cooper, M. J. O. Deegan, A. J. Dobbyn, F. Eckert, E. Goll, C. Hampel, A. Hesselmann, G. Hetzer, T. Hrenar, G. Jansen, C. Köppl, Y. Liu, A. W. Lloyd, R. A. Mata, A. J. May, S. J. McNicholas, H. Meyer, M. E. Mura, A. Nicklass, D. P. O'Neill, P. Palmieri, D. Peng, K. Pflüger, R. Pitzer, M. Reiher, T. Shiozaki, H. Stoll, A. J. Stone, R. Tarroni, T. Thorsteinsson, M. Wang, in: 2012.
[34] Y. Georgievskii, J. A. Miller, M. P. Burke, S. J. Klippenstein, *J. Phys. Chem. A* **117** (46) (2013) 12146-54.
[35] E. Wilhelm, R. Battino, *J. Chem. Phys.* **55** (8) (1971) 4012-&.
[36] H. J. Curran, P. Gaffuri, W. J. Pitz, C. K. Westbrook, *Combust. Flame* **114** (1-2) (1998) 149-177.
[37] D. J. M. Ray, D. J. Waddington, *Combust. Flame* **20** (3) (1973) 327-334.
[38] D. J. M. Ray, A. Redfearn, D. J. Waddington, *Journal of the Chemical Society, Perkin Transactions 2* 10.1039/p29730000540 (5) (1973) 540-543.